RSC Advances

PAPER

View Article Online
View Journal | View Issue



Cite this: *RSC Adv.*, 2025, **15**, 6032

# ZnO functionalized paraffin/diatomite phase change material and its thermal management mechanism in PDMS coatings†

Xinye Liu,‡ Xueyan Hou,‡ Longxin Yan, Yuqi Zhang * and Ji-Jiang Wang

The functionalization of conventional diatomite/paraffin phase change materials is of great significance to expand its application in thermal management. Herein, a nano-ZnO functionalized paraffin/diatomite phase change material (PA/F-DE/ZnO) with enhanced thermal conductivity, anti-leakage and UV-adsorption was prepared by simple melt blending and adsorption. The results indicated that when nano-ZnO was introduced to $PA_1$/F-DE (mass ratio is 1 : 1) system, the obtained PA/F-DE/ZnO not only possessed enhanced thermal conductivity and reduced leakage but also presented excellent UV absorption performance and retained the heat storage performance well. The thermal conductivity of $PA_1$/F-DE/$ZnO_{10}$ (with 10 wt% of ZnO) is enhanced by 87.73% compared with that of PA/F-DE and exhibit high enthalpy of 76 J $kg^{-1}$. Finally, a thermal management PDMS-$PA_1$/F-DE/$ZnO_{10}$ film was constructed by combined 5 wt% $PA_1$/F-DE/$ZnO_{10}$ with Polydimethylsiloxane (PDMS). The surface temperature of PDMS-$PA_1$/F-DE/$ZnO_{10}$ film was 5–6 °C lower than that of PDMS film in the heating temperature range from room temperature to 60 °C, indicating a cooling performance and good thermal stability. The PDMS-$PA_1$/F-DE/$ZnO_{10}$ showed an outstanding cooling for the exothermic computer and phone and usability of the phone in cold conditions. The multiple heat weakening transfer mechanisms such as thermal absorption of PA and thermal reflection of F-DE/ZnO were proposed.

Received 11th November 2024
Accepted 18th February 2025

DOI: 10.1039/d4ra08017c

rsc.li/rsc-advances



## Introduction

Facing severe energy crisis and environmental problems during the rapid development process of social economy, energy conversion and conservation has become a global issue.[1–3] To address these issues, phase change energy storage technology has attracted much attention. Phase change materials (PCMs) can absorb and release heat through the phase transition at a specific temperature, and have been widely used in many fields such as solar heat collection,[4] electronic device heat dissipation,[5,6] building insulation,[7] cold chain transportation,[8] and air conditioning cold storage.[9] The development of efficient functionalized thermal management PCMs is an urgent demand for their practical applications.

As a typical organic PCM, paraffin (PA) has been widely applied due to its high heat storage density, excellent thermo-chemical stability and high phase change latent heat.[10–12] The present research is the focus on the improvement of the anti-leakage of PA. PA encapsulated by inorganic porous materials is an effective and simple method to solve the problems of leakage and instability of PCMs. Porous materials such as diatomite (DE) and other mineral clays,[13,14] graphite and its derivatives,[15–17] and metal foam,[18–20] can be employed as carriers for PCMs.[21,22] Among these porous materials,[23] DE has been widely used attributed to its wide range of sources,[24] low cost, rich pore structure, excellent thermal and chemical stability.[25–28] For example, Zhang *et al.* reported a hydrophobically modified DE using 1*H*,1*H*,2*H*,2*H*-perfluorodecyl trethoxysilane.[29] The encapsulation rate of the modified PA/DE composite was 84.5%, and the PA/DE composite still had good thermal stability after 50 cycles of thawing and freezing. Guo *et al.* prepared PA/DE/wood powder/high-density polyethylene composite PCMs using wood powder/high-density polyethylene as the secondary packaging material to reduce leakage.[30] The composite materials showed good heat storage capacity and temperature regulation ability.

It is desirable to improve the thermal conductivity and multifunction for PA/DE composite PCMs in practical application. Zinc oxide (ZnO) is a metal oxide with a wide conductive band gap of 3.37 eV, showing the advantages of UV absorption, anti-bacteria, non-toxic, low price and environmental friendliness.[31,32] It is a commonly used functional enhancement material for composite materials, and has important applications in solar cells,[33] photocatalysis,[34] and anti-ultraviolet functional coatings or paints.[35,36] The thermal conductivity of nano-ZnO is up to 1.160 W $m^{-1}$ $K^{-1}$. Hence, it can be used to

*College of Chemistry and Chemical Engineering, Yan'an University, Yan'an, Shaanxi 716000, P. R. China. E-mail: yqzhang@iccas.ac.cn*

† Electronic supplementary information (ESI) available. See DOI: https://doi.org/10.1039/d4ra08017c

‡ These authors contributed equally.

improve the thermal conductivity of organic PCMs. For example, Sahan *et al.* prepared PA-ZnO nanotube composites, whose phase transition temperature was basically consistent with that of PA, but the heat storage capacity was slightly reduced.[37] Tong *et al.* prepared Zn–ZnO/PA composite PCMs through a two-step method to improve the thermal conductivity, specific heat capacity, and the photothermal properties of the composites.[38] Presently, most of the porous materials are mainly developed to reduce the leakage of PCMs. It is suggested that ZnO and phase change composites have potential applications in thermal conductivity enhancement and ultraviolet (UV) absorption. The combination of thermal management and UV absorption property of PCMs will expand its application prospects in anti-aging coatings, such as functional textile coatings or building paints that are exposed to the sun require UV absorption to endow the materials with UV-shielding property and favour its resistance to light aging.[39] Zhou *et al.*[40] prepared a bifunctional nano encapsulated PCMs for thermal energy storage and UV absorption, showing a good promise in the applications of intelligent thermoregulation fabrics. However, there are few reports on paraffin/diatomite PCMs combined anti-leakage, thermal conductivity and UV absorption by a simple method.

In this work, we used ZnO as a functional additive to enhance the thermal conductivity, anti-leakage and UV-absorption of paraffin/diatomite PCMs by a simple melt blending and adsorption method. PA was used as the phase change material, cheap and readily available DE acted as carrier, and nano-ZnO contributed the thermal conductivity and UV absorption characteristic. The prepared composite PCMs not only showed enhanced thermal conductivity and low leakage, but also realized the double function of heat storage and UV absorption. A thermal management PDMS-$PA_1$/F-DE/$ZnO_{10}$ film was fabricated by blending the $PA_1$/F-DE/$ZnO_{10}$ and PDMS, achieving a cooling effect of 5 $\sim$ 6 °C in the range of 60 °C. The prepared PDMS-$PA_1$/F-DE/$ZnO_{10}$ film was used on the computers and phones, demonstrating good endothermic and exothermic performance, achieving the cooling for the exothermic devices and usability of the devices in cold conditions. The multiple thermal management mechanism of $PA_1$/F-DE/$ZnO_{10}$ in PDMS coatings were proposed.

## Experimental section

### Materials

Paraffin (PA, RT35) was purchased from Guangzhou Zhongjia New Material Technology Co., Ltd. Diatomite (DE) was obtained from Hefei Bomei Biotechnology Co., Ltd. 1*H*,1*H*,2*H*,2*H*-perfluorodecyl trimethoxy-silane (FAS-17) was provided by Shanghai Maclin Biochemical Technology Co., Ltd. Nano-ZnO (20 nm, 99.9%) was bought from Bosworth Nanotechnology Co., Ltd. Polydimethylsiloxane (PDMS, including prepolymer A and curing agent B) was supplied by Suzhou Haidei Electronic Technology Co., Ltd. Hydrochloric acid (37 wt%) was bought from Sinopod Group Chemical Reagent Co., Ltd. Anhydrous ethanol (AR) came from Tianjin Zhiyuan Chemical Reagent Co., Ltd.

### Preparation of PA/F-DE/ZnO

**Pretreatment of DE.** DE was first calcined in Muffle furnace at 400 °C for 3 h, then soaked in 10 wt% HCl solution at 60 °C for 48 h, followed by rinsing several times with distilled water and drying at 60 °C for 24 h. The dried DE was soaked in ethanol solution containing 1 wt% FAS-17 for 48 h companying with stirring, and then dried at 45 °C. Subsequently, the dried DE was placed in an oven at 220 °C for 5 min, in which FAS-17 completely reacted with DE to obtain hydrophobic modified DE (F-DE).

The PA/F-DE/ZnO composite PCMs were prepared by melt blending and adsorption method. PA was melted at 85 °C in an oven, followed by adding F-DE and melt blending for 4 h. Various PA/F-DE composites were obtained by changing the mass ratios of PA to F-DE (0.5 : 1, 1 : 1, 2 : 1 and 3 : 1). The corresponding samples were labeled as $PA_{0.5}$/F-DE, $PA_1$/F-DE, $PA_2$/F-DE and $PA_3$/F-DE, respectively. Then, different contents of nano-ZnO (1 wt%, 5 wt% and 10 wt% based on the total mass of PA and F-DE) were mixed with PA and F-DE (mass ratio 1 : 1) and melt blending in an oven at 85 °C for 2 h to prepare composite PCMs containing nano-ZnO. The resulting samples were denoted as $PA_1$/F-DE/$ZnO_1$, $PA_1$/F-DE/$ZnO_5$ and $PA_1$/F-DE/$ZnO_{10}$, respectively.

### Application of $PA_1$/F-DE/$ZnO_{10}$

The PDMS prepolymer A (8.0 g) and $PA_1$/F-DE/$ZnO_{10}$ (1.6 g) were mechanically stirred to mix well. Then 0.8 g of curing agent B was added and uniformly mixed and heated to 35 °C for 10 min with stirring. The mixture was poured into a Petri dish and ultrasounded for 20 min at room temperature. The PDMS-$PA_1$/F-DE/$ZnO_{10}$ composite film was obtained after curing at room temperature for 48 h. A PDMS film without $PA_1$/F-DE/$ZnO_{10}$ was prepared by the same method.

The PDMS-$PA_1$/F-DE/$ZnO_{10}$ composite film and the PDMS film were placed on a hot computer or phone and a thermal infrared imager was used to record the temperature change. The heat dissipation performance of PDMS-$PA_1$/F-DE/$ZnO_{10}$ composite film was investigated.

### Characterization and methods

The morphologies of PA/F-DE/ZnO were measured by scanning electron microscope (SEM, Germany ZEISS Sigma 300), and the distribution of ZnO in PCMs was analyzed by energy dispersion spectrometer (EDS). The adsorption–desorption curve and BET specific surface area of DE and F-DE were tested by automatic specific surface and porosity analyzer (America Micromeritics 3Flex). Degassing was performed at 200 °C for 6 h, and $N_2$ was used as the adsorption–desorption test. The chemical composition of the composite PCMs was characterized by Fourier infrared spectrometer (FTIR, Thermo Scientific Nicolet iN10) in the range of 500–4000 $cm^{-1}$ through a resolution of 10 $cm^{-1}$ by KBr tablet method. X-ray diffractometer (XRD, Japanese Rigaku SmartLab SE type) was used to analyze the structural phase and the crystal lattices of phase change composites. The diffraction forms were noted within the diffraction angle ($2\theta$) from 10 to

80°. Differential scanning calorimeter (DSC, Germany DSC200F3) was used to test the phase change performance parameters of PCMs. All samples were heated from 0 to 70 °C with $N_2$ gas flow rate at 5 °C $min^{-1}$ and then cooled down to 0 °C again. The composite PCMs samples were tested by using a thermogravimetric analyzer (TG, NETZSCH STA 449 F5) to characterize the thermal stability.

**Step cooling curve.** The sample was put into a test tube and placed in water bath at 70 °C. After the sample temperature stabilized, the tube with sample was transferred to water bath at 25 °C for cooling. The temperature change of the sample during heating and cooling process was recorded.

**Leakage rate.** Diffusion–permeation ring method was used to test the leakage rate of the composite PCMs. The composite PCMs sample ($m_0$) was pressed into a disc with a diameter of 18 mm and placed on a circular filter paper (the quality of filter paper was $m_2$) with a diameter of 110 mm. Then the filter paper with sample was placed in an oven at 50 °C for different time, followed by removal of the sample and weighing the quality of the filter paper ($m_1$). The leakage rate was calculated according to formula (1). Three parallel samples were used in the measurements for each leakage rate.

$$\text{Leakage rate} = \frac{m_1 - m_2}{m_0} \times 100\% \quad (1)$$

**Thermal infrared imaging.** 0.5 g composite PCMs was pressed into a round sheet and heated on a platform at 50 °C, and the temperature was recorded with a thermal infrared imager at an interval of 120 s. PDMS film and PDMS-$PA_1$/F-DE/$ZnO_{10}$ composite film were heated on a platform at 60 °C and then cooled down at room temperature. The thermal infrared imager was used to take photos, and the temperature of the film surface was recorded with a temperature recorder. The PDMS film and PDMS-$PA_1$/F-DE/$ZnO_{10}$ composite film were placed on the back of a computer or a phone, and the thermal infrared photos were taken during the heat dissipation process.

**Thermal infrared imaging.** 0.5 g composite PCMs was pressed into a round sheet and heated on a platform at 50 °C, and the temperature was recorded with a thermal infrared imager at an interval of 60 s. PDMS film and PDMS-$PA_1$/F-DE/$ZnO_{10}$ composite film were heated on a platform at 50 °C and then cooled down at room temperature. The thermal infrared imager was used to take photos, and the temperature of the film surface was recorded with a temperature recorder. As control, the temperature of films in the dark condition was recorded.

The PDMS film and PDMS-$PA_1$/F-DE/$ZnO_{10}$ composite film were placed on the back of a computer or a phone, and the thermal infrared images were taken during the heat dissipation process. To verify the temperature-regulating performance of the PDMS-$PA_1$/F-DE/$ZnO_{10}$ on phones under cold conditions, the phone was placed in 0 °C refrigerator and frozen for 5 min. Then, a PDMS film and PDMS-$PA_1$/F-DE/$ZnO_{10}$ composite film at 30 °C were placed on the back surface of the phone, and infrared thermal imaging was used to take pictures.

# Results and discussion

### Pretreatment of DE and characterization

Natural DE is a kind of superhydrophilic porous material, which is not compatible with hydrophobic PA well. In order to improve the affinity between DE and PA, DE was modified by FAS-17 to improve its hydrophobicity. Fig. 1a and b show the water contact angle (CA) photos of DE and FAS-17 modified F-DE, respectively. Water droplet quickly permeate on the surface of DE with a CA of 0°, while the CA of F-DE is 136.5°, indicating the successfully hydrophobic treatment for DE. The hydrophobicity of F-DE can provide interfacial action for the absorbing and binding of F-DE and PA. The XRD patterns (Fig. 1c) show the same characteristic peaks at 2$\theta$ of 21.87° and 36.05° for DE and F-DE, indicated that the structure of DE has not been changed after pretreatment by FAS-17.

Nitrogen adsorption test was used to investigate the pore structure of DE before and after pretreatment. Fig. 1d shows the $N_2$ adsorption/desorption isotherms of DE and F-DE. According to the IUPAC adsorption isotherm system, the adsorption curve of DE conformed to type-IV isotherm and type-H3 hysteresis loop occurs, demonstrating a loose hierarchical porous structure with mesoporous structure (2 ~ 50 nm) before and after modification of FAS-17.[41] When relative pressure ($p/p_0$) ranges from 0.2 to 0.9, the isotherm increased rapidly, indicating that there were mesoporous in DE. When $p/p_0$ was greater than 0.9, the isotherms did not appear platform regardless of DE and F-DE. The result indicated that the DE also contained large pore structures (greater than 50 nm), which may be irregular pores formed after the aggregation of DE particles.[42] The pore size of DE and F-DE (Fig. 1e) was distributed in the range of 0 ~ 50 nm. Table 1 shows that the BET surface area, total pore volume and average pore diameter of DE were 0.8499 $m^2$ $g^{-1}$, 0.001185 $cm^3$ $g^{-1}$ and 6.5018 nm, respectively. For F-DE, BET surface area, total pore volume and average pore diameter of F-DE increased to 1.3554 $m^2$ $g^{-1}$, 0.001787 $cm^3$ $g^{-1}$ and 8.9058 nm, respectively. The increased specific surface area and pore diameter of F-DE will provide space for PA adsorption and are conducive to the composite of PA and F-DE.

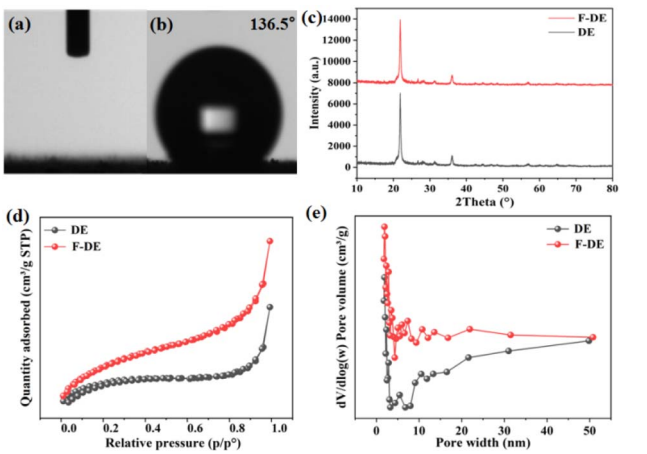


Fig. 1 CA photos of DE (a) and F-DE (b), XRD spectra (c), $N_2$ adsorption/desorption isotherms (d) and pore width distribution curves (e).

Table 1 The porosity parameters of the DE and F-DE

| Samples | BET surface area ($m^2\ g^{-1}$) | Total pore volume ($cm^3\ g^{-1}$) | Mean aperture (nm) |
|---|---|---|---|
| DE | 0.8499 | 0.001185 | 6.5018 |
| F-DE | 1.3554 | 0.001787 | 8.9058 |

## Preparation and characterization of PA/F-DE/ZnO composite PCMs

The preparation process of PA/F-DE/ZnO composite PCMs is shown in Fig. 2. First, DE was hydrophobically treated with FAS-17 to improve its compatibility with PA. Then, different amounts of nano-ZnO were introduced into the system with 1 : 1 mass ratio of PA to F-DE by melt blending and adsorption method. The abundant pores of F-DE were conducive to the adsorption of PA and nano-ZnO on F-DE. The microstructure of F-DE and ZnO was engineered like a 3D network, which was more beneficial for the entrance of PA chains. The melted PA was absorbed into the pores and network by the capillary force.[43] Part of nano-ZnO particles were also adhered to the surface and pores of F-DE together with PA, forming the PA/F-DE/ZnO composite PCMs. The encapsulation of PA in F-DE pore and stabilized by nano-ZnO particles was beneficial to preventing PA leakage during the phase transition process, giving PA efficient heat storage performance. The excellent thermal conductivity and UV absorption properties of nano-ZnO were utilized to enhance and enrich the properties of composite PCMs. In addition, ZnO nanoparticles can limit the fluidity of PA in the phase change melting process at a certain extent, which is helpful to reduce the leakage of PA.

To prepare the optimal PA/F-DE/ZnO composite PCMs, the effect of mass ratio between PA and F-DE on the properties of PA/F-DE were investigated. The structure and phase transition temperature-control properties of PA/F-DE were characterized by XRD spectra (Fig. S1†), DSC (Fig. S2†), step cooling (Fig. S3†) and leakage rate (Fig. S4†). The results indicated that when the mass ratio of PA to F-DE was 1 : 1, the leakage rate of $PA_1$/F-DE was obviously reduced and the phase transition enthalpy was higher.

Then, different contents of nano-ZnO were introduced into the $PA_1$/F-DE system. XRD was performed on PA, $PA_1$/F-DE and $PA_1$/F-DE/ZnO composites, as shown in Fig. 3a.[44] It can be seen that two sharp diffraction peaks at 2$\theta$ of 21.4° and 24.0° of PA can be observed in PA and $PA_1$/F-DE. The characteristic peaks at 31.76°, 34.41°, 36.24° of ZnO can be found in $PA_1$/F-DE/ZnO composites,[45] and the intensity increased with increasing ZnO contents.[44] The FTIR spectra of PA, $PA_1$/F-DE and $PA_1$/F-DE/ZnO in Fig. 3b show that $PA_1$/F-DE and $PA_1$/F-DE/ZnO had the characteristic peaks of PA. Comparing PA1/F-DE and $PA_1$/F-DE/ZnO, we can find that a broad absorption peak at 3440 $cm^{-1}$ appeared, which can be attributed to the –OH vibration of ZnO.[46] The band between the 430 and 550 $cm^{-1}$ was associated to Zn–O bonds. Furthermore, the intensity of these two peaks enhanced with the increasing ZnO contents. Furthermore, no new peaks appeared in the XRD and FT-IR were found for $PA_1$/F-DE/ZnO, indicating no chemical reaction occurred. PA, F-DE and ZnO were combined successfully by physical interaction.

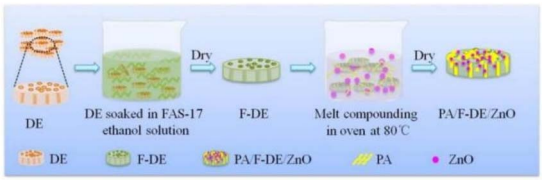


Fig. 2 Schematic illustration of the preparation for PA/F-DE/ZnO composite PCMs.

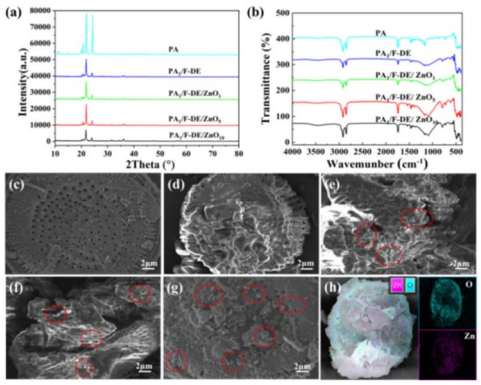


Fig. 3 XRD (a) and FTIR (b) of PA and PA/F-DE/ZnO composite PCMs, SEM images of F-DE (c), $PA_1$/F-DE (d), $PA_1$/F-DE/$ZnO_1$ (e), $PA_1$/F-DE/$ZnO_5$ (f), $PA_1$/F-DE/$ZnO_{10}$ (g), and EDS of $PA_1$/F-DE/$ZnO_{10}$ (h).

To intuitively illustrate the microstructure, SEM of F-DE, $PA_1$/F-DE and $PA_1$/F-DE/ZnO composite PCMs was performed and shown in Fig. 3c–g. The clear pore structure of F-DE (Fig. 3c) indicated that the impurities in DE had been removed cleanly after successive high-temperature calcination, HCl treatment and FAS-17 modification. The porous F-DE can provide more space to adsorb and package PA. Compared with F-DE, the surface and pores of $PA_1$/F-DE (Fig. 3d) were covered by or partially filled with PA, and resulted in reduced pore size, indicating that PA has been successfully adsorbed.[44] After introducing nano-ZnO into $PA_1$/F-DE, solid particles (circled in the SEM image) appeared on the surface of $PA_1$/F-DE/ZnO (Fig. 3e–g). The number of particles increased with increasing ZnO contents, especially for $PA_1$/F-DE/$ZnO_{10}$ with 10 wt% of ZnO (Fig. 3g). To further verify the composition of these particles, the distribution of Zn and O elements on $PA_1$/F-DE/$ZnO_{10}$ surface was performed by EDS (Fig. 3h). The results demonstrate that Zn and O elements were uniformly distributed on the surface of $PA_1$/F-DE/$ZnO_{10}$, which was consistent with the position of solid particles. Therefore, nano-ZnO was well dispersed in $PA_1$/F-DE/ZnO, testifying successful combination of ZnO and PA/F-DE.

## Thermal properties of $PA_1$/F-DE/ZnO composite PCMs

**Thermal storage properties of $PA_1$/F-DE/ZnO.** Fig. 4(a and b) provide the DSC curves of PA, $PA_1$/F-DE and $PA_1$/F-DE/ZnO composite PCMs during endothermic (Fig. 4a) and exothermic

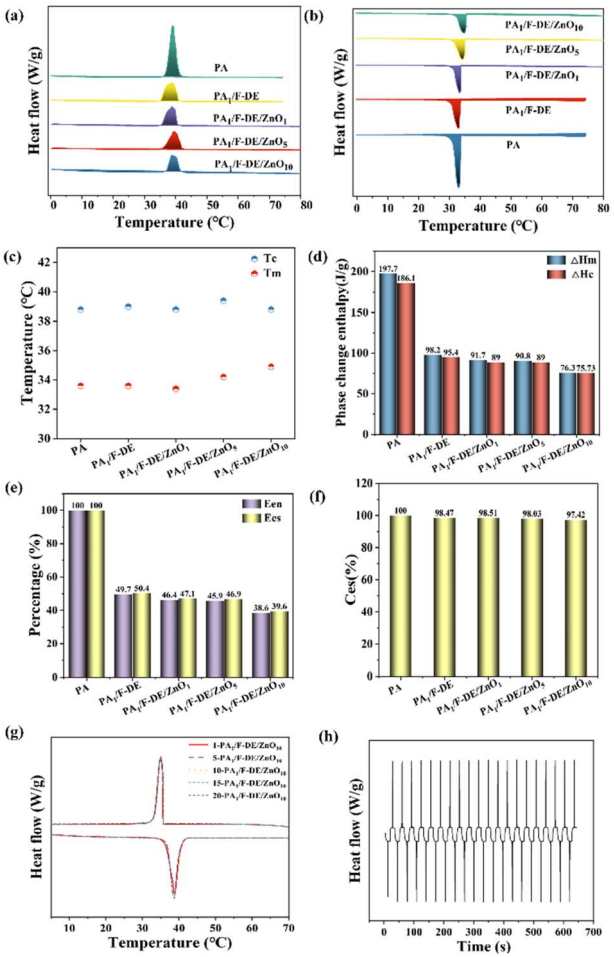


Fig. 4 DSC curves of PA, $PA_1$/F-DE and $PA_1$/F-DE/ZnO during endothermic (a) and exothermic (b) processes, and their melting ($T_m$) and crystallization temperature ($T_c$) (c), phase change enthalpy (d), encapsulation rate ($E_{en}$), encapsulation efficiency $E_{es}$ (e) and thermal storage efficiency $C_{es}$ (f), and DSC curves of $PA_1$/F-DE/$ZnO_{10}$ after experiencing 20 heating–cooling cycles (g and h).

(Fig. 4b) processes. PA had strong endothermic and exothermic peaks, and the similar peaks can be observed for $PA_1$/F-DE and $PA_1$/F-DE/ZnO. This indicates that the thermal behavior of the PA1/F-DE and PA1/F-DE/ZnO PCMs was similar to that of PA, which can store heat or control temperature by absorbing and releasing heat to phase transition. As shown in Fig. 4c, the melting ($T_m$) and crystallization temperature ($T_c$) of $PA_1$/F-DE and $PA_1$/F-DE/ZnO were close to those of PA. The phase change temperature of PA has not been affected after shaped by F-DE and ZnO. This may be due to the fact that PA was adsorbed on F-DE only by physical interaction without chemical effects, which can be supported by the data from FTIR and XRD. The $\Delta H_m$ and $\Delta H_c$ of $PA_1$/F-DE (Fig. 4d) were 98.2 J $kg^{-1}$ and 95.4 J $kg^{-1}$, which were about 50% of the PA (197.7 J $kg^{-1}$ of $\Delta H_m$ and 186.1 J $kg^{-1}$ of $\Delta H_c$). This was close to the theoretical mass fraction of PA in $PA_1$/F-DE (the mass ratio of PA to F-DE was 1 : 1), indicating that PA in $PA_1$/F-DE still maintained the similar phase transition performance as pure PA. The thermal performance of PA has not been reduced after encapsulated by F-DE.

The $\Delta H_m$ and $\Delta H_c$ of $PA_1$/F-DE/ZnO decreased slightly with increasing ZnO contents. This is because the presence of the ZnO reduced the weight fraction of PA in the $PA_1$/F-DE/ZnO composite system, and the corresponding phase transition enthalpy decreased with increasing ZnO contents. The encapsulation rate ($E_{en}$), encapsulation efficiency ($E_{es}$) and thermal storage efficiency ($C_{es}$) of the composite PCMs were calculated by eqn (2)–(4), and the results are shown in Fig. 4e and f.[47] Both $E_{en}$ and $E_{es}$ were close to the theoretically calculated contents of PA in the composite PCMs, indicating the phase change heat storage capacity of PA has been well preserved after encapsulation of F-DE and ZnO. This can be attributed to the abundant pore structure and hydrophobic surface treatment of F-DE. The hydrophobic surface improves the compatibility between PA and F-DE, and the porous structure provides enough porous space for the adsorption of PA. Fig. 4f shows that the $C_{es}$ of all $PA_1$/F-DE/ZnO composite PCMs were greater than 97%, showing good phase change thermal storage performance. The latent heat of prepared $PA_1$/F-DE/ZnO is superior to that of similar materials with paraffin and diatomite in existing literature (Table S1†).[29,48] Moreover, due to the introduction of ZnO, its thermal conductivity was enhanced and UV absorption property was imparted. Thus, it has more advantages in the application of anti-ultraviolet requirements thermal management.

$$E_{en}(\%) = \frac{\Delta H_{m,M}}{\Delta H_{m,PA}} \times 100\% \quad (2)$$

$$E_{es}(\%) = \frac{\Delta H_{m,M} + \Delta H_{c,M}}{\Delta H_{m,PA} + \Delta H_{c,PA}} \times 100\% \quad (3)$$

$$C_{es}(\%) = \frac{E_{es}}{E_{en}} \times 100\% \quad (4)$$

where $\Delta H_{m,M}$ and $\Delta H_{c,M}$ represent the enthalpies of melting and crystallization of the composite PCMs, and $\Delta H_{m,PA}$ and $\Delta H_{c,PA}$ are the enthalpies of melting and crystallization of PA.

The DSC curves of $PA_1$/F-DE/$ZnO_{10}$ after experiencing 20 heating–cooling cycles are shown in Fig. 4g and h. The thermal property of $PA_1$/F-DE/$ZnO_{10}$ after experiencing 20 heating–cooling cycles are listed in Table 2. The results indicated that the phase change temperature did not change obviously. $\Delta H_m$ and $\Delta H_c$ of the $PA_1$/F-DE/$ZnO_{10}$ after experiencing 20 heating–cooling cycles did not decrease. This illustrated that $PA_1$/F-DE/$ZnO_{10}$ has a highly stable phase change property during the continuous cyclic processes of heat storage and release.

Table 2 Thermal property of $PA_1$/F-DE/$ZnO_{10}$ after experiencing 20 heating–cooling cycles

| | Endothermic process | | Exothermic process | |
|---|---|---|---|---|
| Samples | $T_m$ (°C) | $\Delta H_m$ (J $g^{-1}$) | $T_c$ (°C) | $\Delta H_c$ (J $g^{-1}$) |
| Cycle 1 | 38.76 | 78.99 | 35.59 | 77.43 |
| Cycle 5 | 38.68 | 76.45 | 35.63 | 76.45 |
| Cycle 10 | 38.71 | 76.69 | 35.67 | 76.34 |
| Cycle 15 | 38.59 | 76.62 | 35.70 | 76.26 |
| Cycle 20 | 38.62 | 76.32 | 35.73 | 76.43 |

The thermal storage and thermal regulation performance of $PA_1$/F-DE/ZnO composite PCMs was measured by step-cooling curves, shown in Fig. 5a. The step-cooling curve of F-DE shows that there was no temperature platform during both heating and cooling. The heating process of PA and composite PCMs can be distinguished into three visible stages. Stage 1: the PA was heated to approximately 34 °C and the heating rate of the $PA_1$/F-DE/ZnO composite PCMs was gradually faster than the PA due to the thermal conductivity of the former was higher than the latter, and the $PA_1$/F-DE/ZnO was in the endothermic state before the solid–liquid phase transition. Therefore, the heating process of $PA_1$/F-DE/ZnO was relatively faster than PA. Stage 2: the temperature ranges from 34 °C to 39 °C (Fig. 5b), which is the phase change temperature of PA. In this stage, both the pure PA and the encapsulated PA undergo the phase transition and maintained the temperature change small and kept for some time forming a temperature platform in this temperature range. The temperature platform held time of the $PA_1$/F-DE/ZnO decreased with an increase in ZnO content. This can be attributed to the good thermal conductivity of ZnO, leading to a fast heat transfer and temperature change of $PA_1$/F-DE/ZnO. The temperature holding time of the PA was greater than that of $PA_1$/F-DE/ZnO composite PCMs due to phase change enthalpy. Stage 3: the temperature ranges from 40 °C to 70 °C, the temperature rose rapidly because melted PA no longer absorbed and stored heat, and the heat absorbed by PA and $PA_1$/F-DE/ZnO was shown as an increase in temperature. As for cooling process, the temperature changes of PA and $PA_1$/F-DE/ZnO composite PCMs also experienced three stages as 70–39 °C, 39 °C to 33 °C and 33 °C to room temperature. The stage from 70 °C to 39 °C showed a rapid drop in temperature in the exothermic state before the liquid–solid phase transition. The stage from 39 °C to 33 °C is the liquid–solid phase transition of PA. In this stage (Fig. 5c), the melted PA released the heat that stored during the heating process and undergoing a liquid–solid phase transition, maintaining an unchanged temperature. The temperatures of $PA_1$/F-DE/ZnO composite PCMs were higher than that of PA and $PA_1$/F-DE, which can be attributed to the enhanced thermal conductivity of ZnO. The stage from 33 °C to room temperature was the process of natural cooling of solid PA with the ambient temperature. Thus, $PA_1$/F-DE/ZnO PCMs retained the phase change temperature-control performance of PA, and the thermal conductivity was improved. The thermal conductivity of PA, F-DE, ZnO and the composite PCMs are shown in Fig. 5d. The thermal conductivity of PA was 0.0519 W $m^{-1}\cdot K^{-1}$. The thermal conductivity of F-DE and ZnO were 0.0819 W $m^{-1}\cdot K^{-1}$ and 0.1256 W $m^{-1}\cdot K^{-1}$, respectively. After introducing ZnO, the thermal conductivity of $PA_1$/F-DE/ZnO composites were improved and the thermal conductivity $PA_1$/F-DE/$ZnO_{10}$ was increased by 87.73% compared with that of PA/F-DE. This should be attributed to the contribution of ZnO and F-DE to the $PA_1$/F-DE/ZnO composite, among which ZnO played a leading role in enhancing thermal conductivity. On the other hand, the bridge effect formed by F-DE and ZnO is conducive to heat transfer in the $PA_1$/F-DE/ZnO composites.

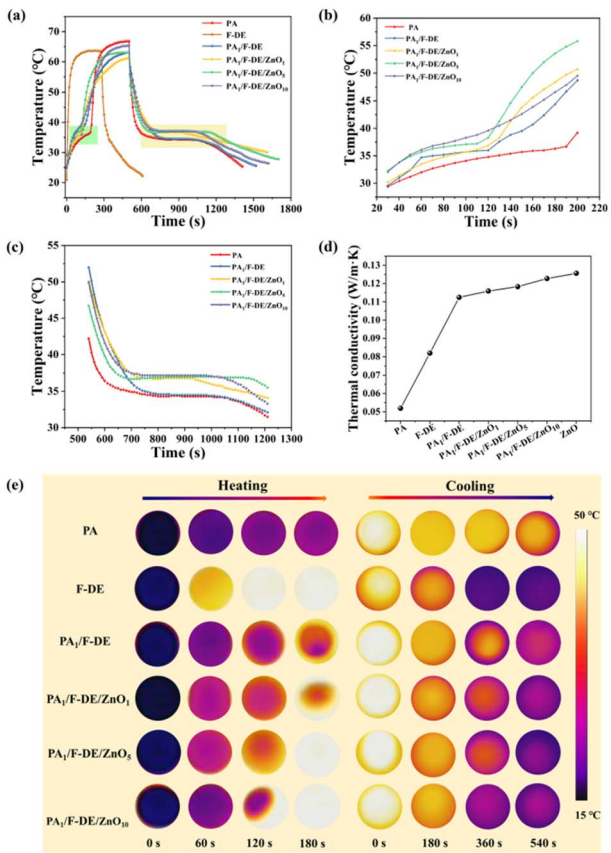


Fig. 5 The step-cooling curves (a) and the corresponding temperature platform in heating (b) and cooling (c), thermal conductivity (d), thermal infrared images in the heating and cooling process (e) of PA, F-DE, $PA_1$/F-DE/ZnO composite PCMs.

Fig. 5e presents the thermal infrared images of PA, F-DE, $PA_1$/F-DE and $PA_1$/F-DE/ZnO composite PCMs during heating and cooling. During heating and cooling, PA exhibited the slowest heating and cooling rates. This is because the phase transition latent heat of pure PA is the largest, and it can absorb and release the most heat through phase transformation under the same condition. However, F-DE showed the fastest temperature changes because it cannot store heat by phase transition to control the temperature. The temperature of $PA_1$/F-DE changed slowly with the extension of heating and cooling time. When the ambient temperature changed, PA in $PA_1$/F-DE composite PCMs underwent phase transformation through the absorption and release of heat, resulting in the slow change of temperature and indicating the temperature-control performance. The temperature changes of $PA_1$/F-DE/ZnO composite PCMs were faster than that of $PA_1$/F-DE due to the good thermal conductivity of ZnO during heating process. Furthermore, the temperature rise rate was accelerated by increasing ZnO content. Compared with the heating process, the temperature variation caused by different ZnO contents was not obvious during cooling process. This is because the heating process is active when samples were put on the constant temperature platform (~50 °C), and the sample temperature changed rapidly. The good thermal conductivity of ZnO promoted the rapid transfer of heat and the temperature change was highly dependent on the ZnO contents. Differently, the cooling process

is natural under room temperature condition. There was little difference in the contribution of ZnO contents to the natural cooling of PCMs. Therefore, the thermal conductivity of ZnO plays a dominant role in the heating process of $PA_1$/F-DE/ZnO PCMs, while it was not obvious for the cooling process. The results demonstrate that the introduction of ZnO was beneficial to the thermal response of $PA_1$/F-DE/ZnO.

**Thermal stability of $PA_1$/F-DE/ZnO.** The leakage rate of $PA_1$/F-DE/ZnO was an important factor to evaluate its stability and application durability. Fig. 6a shows the leakage rate of $PA_1$/F-DE/ZnO composite PCMs obtained by the leakage experiment at 50 °C for different time. The leakage rate of $PA_1$/F-DE, $PA_1$/F-DE/$ZnO_1$ $PA_1$/F-DE/$ZnO_5$ and $PA_1$/F-DE/$ZnO_{10}$ at 60 min were 4.03, 4.0, 3.92, 3.74%, respectively. It can be seen that when ZnO was introduced, the leakage rates of $PA_1$/F-DE/ZnO were reduced with the increasing of ZnO contents. Compared with $PA_1$/F-DE, the leakage rate of $PA_1$/F-DE/$ZnO_{10}$ reduced by 7.2%. It also can be observed intuitively from the diffusion-permeation ring of the samples on the filter paper (Fig. 6b) after heating at 50 °C for 60 min. PA melted and diffused to form the largest seepage ring. The diffusion–permeation rings of $PA_1$/F-DE and $PA_1$/F-DE/ZnO were smaller and $PA_1$/F-DE/$ZnO_{10}$ formed the smallest ring, which was consistent with the leakage rate.[49] The reduction of leakage rate should be attributed to the porous structure of F-DE and the barrier of ZnO nanoparticles. The preventing leakage mechanism of $PA_1$/F-DE/ZnO is shown in Fig. 6c. While PA melting in PA/F-DE/ZnO composites, melted PA was tightly confined in the F-DE framework due to surface tension and capillary force.[50] As solid nanoparticles with high specific surface area, ZnO also adsorb PA and play a barrier role to limit the fluidity of melted PA. The hybrid composites carrier composed of F-DE and ZnO nanoparticles possess approving shape stability. Microstructure of F-DE and ZnO is engineered like a 3D network, which is more beneficial for the entrance of PA chains compared to single F-DE pores. The microstructure is significantly influential on the movement of PA molecular chains. It should be highlighted that the synergistic effect of F-DE and ZnO makes an important contribution to the preventing leakage of $PA_1$/F-DE/ZnO composites. The thermal stability of the material can also be proved by TG in Fig. S5.† Compared with PA, the decomposition temperature of the $PA_1$/F-DE/ZnO composite PCMs was higher, indicating that the stability was improved by F-DE and ZnO.

In addition to the outstanding heat storage and thermal conductivity, the introduction of ZnO makes $PA_1$/F-DE/ZnO have a certain UV resistance.[51,52] Fig. S6† indicated that $PA_1$/F-DE/ZnO present a UV absorption property and the absorption intensity increased with the increasing ZnO contents. The UV adsorption of $PA_1$/F-DE/ZnO PCMs will provide a good application prospect in anti-aging coatings, such as functional textile coatings or building paints that are exposed to the sun and require UV absorption properties to improve their aging resistance.[53]

**Application of PA/F-DE/ZnO in the cooling of PDMS film.** $PA_1$/F-DE/$ZnO_{10}$ was blended with PDMS and the resultant film (PDMS-$PA_1$/F-DE/$ZnO_{10}$) was used to investigate the thermal management in electronic products.[54,55] Fig. 7a shows the photographs of PDMS (sample 1) and PDMS-$PA_1$/F-DE/$ZnO_{10}$ (sample 2) films and their coatings on glass substrates. The PDMS-$PA_1$/F-DE/$ZnO_{10}$ still formed good film. PDMS and PDMS-$PA_1$/F-DE/$ZnO_{10}$ films were heated on a 60 °C heating platform and then naturally cooled at room temperature. Their temperature changes were monitored, as shown in Fig. 7b. In the range from room temperature to 60 °C, the surface temperature of PDMS-$PA_1$/F-DE/$ZnO_{10}$ was lower 5 ∼ 6 °C than that of PDMS during the whole heating process (0 ∼ 260 s) and the initial cooling stage (260 ∼ 380 s). This can be attributed to the phase change and temperature-control performance of $PA_1$/F-DE/$ZnO_{10}$. The temperature of PDMS-$PA_1$/F-DE/$ZnO_{10}$ film was controlled to slowly rise by absorbing heat based on the phase transformation of PA. To compare the influence of light on temperature of PDMS-$PA_1$/F-DE/$ZnO_{10}$, the temperature of films under dark condition was also tested (Fig. S7†). The results demonstrate that light has little effect on the surface temperature of the PDMS-$PA_1$/F-DE/$ZnO_{10}$. The temperature change of PDMS-$PA_1$/F-DE/$ZnO_{10}$ film mainly depends on the

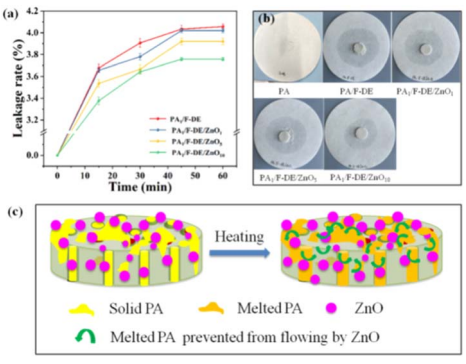


Fig. 6 The leakage rate (a), the photos of diffusion–permeation ring on the filter paper for 60 min (b) and the preventing leakage mechanism (c) of $PA_1$/F-DE/ZnO composite PCMs.

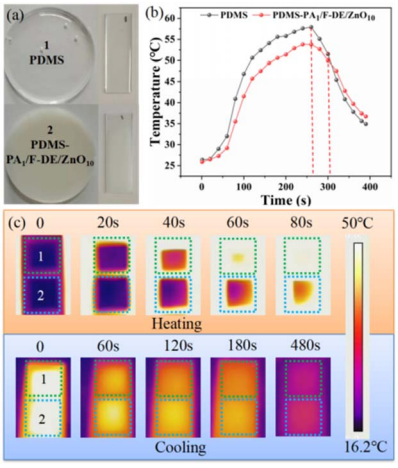


Fig. 7 Photographs of PDMS and PDMS-$PA_1$/F-DE/$ZnO_{10}$ films and coatings on glass substrates (a), the temperature changes of film surface during heating and cooling with time (b) and thermal infrared images (c).

properties of $PA_1$/F-DE/$ZnO_{10}$. On the other hand, we found that the appearance of PDMS-$PA_1$/F-DE/$ZnO_{10}$ film did not change in the heating process, and there was no leakage of melting PA. This is because the encapsulation of PA by F-DE and ZnO limited the flow of molten PA in the composite PCMs, improving the stability of PA. Therefore, the PDMS-$PA_1$/F-DE/$ZnO_{10}$ had good thermal stability.

The infrared thermal images in Fig. 7c visually present the temperature of PDMS film rised rapidly after heating for 40 s and reached above 50 °C at 80 s. On the contrary, the temperature of PDMS-$PA_1$/F-DE/$ZnO_{10}$ increased slowly. The temperature was around 27 °C at 40 s and was below 50 °C at 80 s in most areas. During the natural cooling process, both the surface temperature of PDMS and PDMS-$PA_1$/F-DE/$ZnO_{10}$ films changed slowly and the temperature of PDMS-$PA_1$/F-DE/$ZnO_{10}$ decreased more slowly than that of PDMS. The results revealed that PDMS-$PA_1$/F-DE/$ZnO_{10}$ had good temperature-control performance. To further demonstrate the stability of $PA_1$/F-DE/$ZnO_{10}$ in the application in PDMS-$PA_1$/F-DE/$ZnO_{10}$ thermal management performance, 10 cycles of heating and cooling of PDMS-$PA_1$/F-DE/$ZnO_{10}$ were carried out, shown in Fig. 8. It can be seen that the temperature change of the PDMS-$PA_1$/F-DE/$ZnO_{10}$ films was slower than that of PDMS both in heating and cooling process, indicating good and stable temperature-control thermal management performance. This can be contributed to the thermal stability of $PA_1$/F-DE/$ZnO_{10}$.This can be attributed to the shaping effect of F-DE and ZnO on PA, which made $PA_1$/F-DE/$ZnO_{10}$ maintain good performance stability in thermal cycles.

In addition, the heat dissipation and cooling effect of PDMS-$PA_1$/F-DE/$ZnO_{10}$ composite film on thermal electronic devices such as computer and phone were studied. PDMS (sample 1) and PDMS-$PA_1$/F-DE/$ZnO_{10}$ (sample 2) were placed on a hot computer (Fig. 9a) and a phone (Fig. 9b), and the temperature changes were observed by thermal infrared imaging. It can be found that the temperature of PDMS-$PA_1$/F-DE/$ZnO_{10}$ film on computer and phone were lower than that of PDMS. This can be attributed to the solid–liquid phase transition of PA in the $PA_1$/F-DE/$ZnO_{10}$, which can absorb the heat emitted by the computer or phone, resulting in a cooling effect for PDMS-$PA_1$/F-DE/$ZnO_{10}$ film on computer and phone. The composite film or coatings containing $PA_1$/F-DE/$ZnO_{10}$ would be expected to alleviate the heat problem of computer and phone during use or charging. In order to verify the heat storage and release performance of PDMS-$PA_1$/F-DE/$ZnO_{10}$ used in cold conditions of phone, we investigated the application of PDMS-$PA_1$/F-DE/$ZnO_{10}$ on a cold phone under simulated cold conditions (Fig. 9c). When the phone was moved from room to cold conditions, the thermal management PDMS-$PA_1$/F-DE/$ZnO_{10}$ coating can keep the phone temperature from falling rapidly with the ambient temperature, indicating the heat release performance of PDMS-$PA_1$/F-DE/$ZnO_{10}$ for phone under cold condition. In this process, we mainly focused on the thermal management performance of our PCMs.

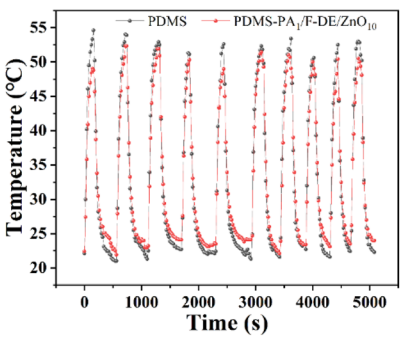


Fig. 8 Temperature changes of PDMS-$PA_1$/F-DE/$ZnO_{10}$ for 10 cycles heating and cooling.

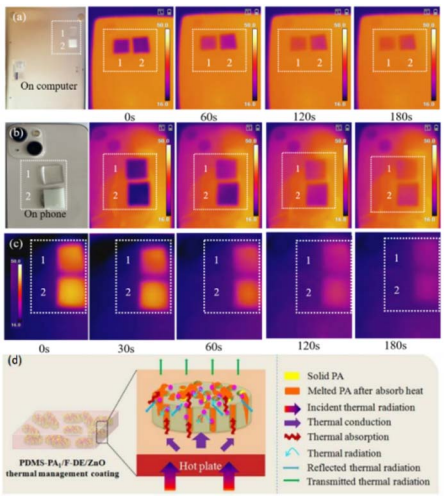


Fig. 9 Infrared thermal images of PDMS (1) and PDMS-$PA_1$/F-DE/$ZnO_{10}$ (2) films placed on the back of a computer (a), a phone (b) and on a cold phone (c), the thermal management mechanism diagram of PDMS-$PA_1$/F-DE/ZnO coating (d).

The thermal management mechanism of PDMS-$PA_1$/F-DE/ZnO film is illustrated in Fig. 9d. The composite film is composed of PDMS matrix and $PA_1$/F-DE/$ZnO_{10}$. When PDMS-$PA_1$/F-DE/ZnO sample is used on heating electronic devices such as phone or computer, the incident thermal radiation produced by phone or computer begins to transfer, conduct and radiate through the composite film. The thermal conduction can be weakened due to the PDMS polymer matrix and $PA_1$/F-DE/ZnO. Most of the heat flow can be absorbed and stored by PA in $PA_1$/F-DE/ZnO as latent heat with a solid–liquid phase transition when the temperature is higher than the melting temperature of PA. The rest heat continues to transfer through the composite film. The thermal transfer and radiation to the external environment can be enhanced by ZnO particles thanks to the good thermal conductivity. In addition, a small part of the heat is reduced by reflection during the conduction process in PDMS, F-DE and ZnO. Compared with PMDS, PDMS-$PA_1$/F-DE/ZnO film presents a comprehensive cooling ability because of the multiple heat weakening transfer, such as thermal absorption of PA phase change transition and thermal transfer, reflection radiation by F-DE and ZnO. Similarly, when the film is used in cold conditions, the PDMS-$PA_1$/F-DE/ZnO composite can release its stored heat, so that the temperature of the phone

does not plummet as the ambient temperature decreases. In this case, F-DE and ZnO also promote the heat transfer from the PDMS-$PA_1$/F-DE/ZnO composite to the phone.

## Conclusions

We developed a nano-ZnO functionalized paraffin/diatomite phase change material (PA/F-DE/ZnO) with enhanced thermal conductivity by simple melt blending and adsorption method. The phase change material PA was encapsulated by hydrophobic treated diatomite and nano-ZnO was used as functional additive to obtained the $PA_1$/F-DE/ZnO PCMs with low leakage rate, good thermal stability and thermal conductivity, and UV absorption function. The results indicated that when nano-ZnO was introduced to $PA_1$/F-DE(mass ratio is 1 : 1) system, the obtained PA/F-DE/ZnO not only possessed enhanced thermal conductivity and reduced leakage but also presented excellent UV absorption performance and retained the heat storage performance well. Compared with PA/F-DE, $PA_1$/F-DE/$ZnO_{10}$ (with 10 wt% of ZnO) exhibit high enthalpy of 76 J $kg^{-1}$, the thermal conductivity was enhanced by 87.73%, leakage rate was reduced by 7.2%. With the best comprehensive performance, $PA_1$/F-DE/$ZnO_{10}$ was blended with PDMS film to obtain a PDMS-$PA_1$/F-DE/$ZnO_{10}$ composite temperature-control film for the thermal management of electronic products. In the temperature range of 60 °C, the PDMS-$PA_1$/F-DE/$ZnO_{10}$ composite film had a cooling effect of 5 $\sim$ 6 °C lower than that of PDMS film, indicating a cooling performance and good thermal stability. The PDMS-$PA_1$/F-DE/$ZnO_{10}$ showed an outstanding cooling for the exothermic computer and phone and usability of the phone in cold conditions. The multiple heat weakening transfer mechanisms such as thermal absorption of PA and thermal reflection of F-DE/ZnO were proposed. The prepared $PA_1$/F-DE/ZnO composite PCMs was expected to be used in thermal management coatings of electronic products, other phase change heat storage and temperature control fields.

## Data availability

The data that support the findings of this study are available within the article and its ESI.†

## Author contributions

Xinye Liu, Xueyan Hou and Yuqi Zhang designed the project; Xinye Liu, Longxin Yan synthesized and characterized the composite PCMs and evaluated the performance, provided suggestions and technical support. Xueyan Hou, Xinye Liu and Yuqi Zhang wrote and edited the manuscript; Ji-Jiang Wang supervised the project.

## Conflicts of interest

There are no conflicts to declare.

## Acknowledgements

The authors thank the National Natural Science Foundation of China (Grant No. 21663032), the Open Sharing Platform for Scientific and Technological Resources of Shaanxi Province (Grant No. 2021PT-004) and Shaanxi Province Key Research and Development Plan (Grant No. 2022GY-412), College Students Innovation and Entrepreneurship Training Program of Yan'an University (Grant No. D2022081, D2023072).

## Notes and references

1 D. Cheng, Y. Li, J. Zhang, M. Tian, B. Wang, Z. He, L. Dai and L. Wang, Recent advances in electrospun carbon fiber electrode for vanadium redox flow battery: Properties, structures, and perspectives, *Carbon*, 2020, **170**, 527–542.
2 P. Yu, H. Yang, X. Chen, Z. Yi, W. Yao, J. Chen, Y. Yi and P. Wu, Ultra-wideband solar absorber based on refractory titanium metal, *Renewable Energy*, 2020, **158**, 227–235.
3 Z. Zhang, L. Zhang, L. Hu and C. Huang, Active cell balancing of lithium-ion battery pack based on average state of charge, *Int. J. Energy Res.*, 2020, **44**, 2535–2548.
4 A. Waseem, M. Khurram, J. Shi, T. Hassina, Z. Liang, U. Ali, W. Guo, X. Huang, W. Wu, R. Yao, Q. Yan and R. Zou, Highly efficient solar-thermal storage coating based on phosphorene encapsulated phase change materials, *Energy Storage Mater.*, 2020, **32**, 199–207.
5 X. Guo and J. Feng, Facilely prepare passive thermal management materials by foaming phase change materials to achieve long-duration thermal insulation performance, *Composites, Part B*, 2022, **245**, 110203.
6 S. Ren and J. Feng, A versatile approach for preparing shape-morphing bilayer films by simply adhering two SEBS/Paraffin films with different deformability and melting temperatures, *Adv. Mater. Technol.*, 2022, **32**, 2200339.
7 A. Can, İ. Özlüsoylu, E. Sözen and M. E. Ergün, Properties of Pinus nigra Arn. wood impregnated with phase change materials for potential energy-saving building material, *J. Energy Storage*, 2024, **83**, 110687.
8 Y. Chen, X. Zhang, J. Ji and C. Zhang, Cold chain transportation energy conservation and emission reduction based on phase change materials under dual-carbon background: a review, *J. Energy Storage*, 2024, **86**, 111258.
9 P. Dhamodharan, A. K. Bakthavatsalam, V. P. Nijin, R. Prabakaran and S. Chul Kim, Enhancing cold storage efficiency: sustainable apple pre-cooling utilizing polyethylene glycol and waste coconut oil as phase change materials for chilled energy recovery from air-conditioning condensate, *Energy*, 2024, **297**, 131296.
10 J. Zhou, H. Fei, Q. He, P. Li, Y. Pan and X. Liang, Structural characteristics and thermal performances of paraffin-based phase change materials for phase change sunshade, *Appl. Phys. A:Mater. Sci. Process.*, 2024, **130**, 196.
11 R. Gulfam, P. Zhang and Z. Meng, Advanced thermal systems driven by paraffin-based phase change materials – a review, *Appl. Energy*, 2019, **238**, 582–611.

12 R. Bharathiraja, T. Ramkumar, M. Selvakumar and N. Radhika, Thermal characteristics enhancement of paraffin wax phase change material (PCM) for thermal storage applications, *Renewable Energy*, 2024, **222**, 119986.
13 R. Wen, X. Zhang, Y. Huang, Z. Yin, Z. Huang, M. Fang and X. Wu, Preparation and properties of fatty acid eutectics/expanded perlite and expanded vermiculite shape-stabilized materials for thermal energy storage in buildings, *Energy Build.*, 2017, **139**, 197–204.
14 C. Li, B. Xie, J. Chen, Z. He, Z. Chen and Y. Long, Emerging mineral-coupled composite phase change materials for thermal energy storage, *Energy Convers. Manage.*, 2019, **183**, 633–644.
15 L. Zhang, S. Wang, G. Yang, H. Luo, H. Lai and T. Liu, Improving freeze resistance of cement-based materials with modified graphite-paraffin composite low-temperature microencapsulated phase change materials, *J. Build. Eng.*, 2024, **90**, 109456.
16 J. Yang, L. S. Tang, R. Y. Bao, L. Bai, Z. Y. Liu, B. H. Xie, M. B. Yang and W. Yang, Hybrid network structure of boron nitride and graphene oxide in shape-stabilized composite phase change materials with enhanced thermal conductivity and light-to-electric energy conversion capability, *Sol. Energy Mater. Sol. Cells*, 2018, **174**, 56–64.
17 N. Şahan and H. Paksoy, Investigating thermal properties of using nano-tubular ZnO powder in paraffin as phase change material composite for thermal energy storage, *Composites, Part B*, 2017, **126**, 88–93.
18 H. Zheng, C. Wang, Q. Liu, Z. Tian and X. Fan, Thermal performance of copper foam/paraffin composite phase change material, *Energy Convers. Manage.*, 2018, **157**, 372–381.
19 B. Yang, Y. Cao, R. Zhang and X. Yu, Experimental investigation on the stability and heat transfer enhancement of phase change materials composited with nanoparticles and metal foams, *J. Energy Storage*, 2024, **89**, 111826.
20 X. K. Yu, Y. B. Tao and Q. Q. Deng, Experimental study on thermal management of batteries based on the coupling of metal foam-paraffin composite phase change materials and air cooling, *J. Energy Storage*, 2024, **84**, 110891.
21 M. Sheikholeslami, Efficacy of porous foam on discharging of phase change material with inclusion of hybrid nanomaterial, *J. Energy Storage*, 2023, **62**, 106925.
22 C. Li, B. Xie, Z. He, J. Chen and Y. Long, 3D structure fungi-derived carbon stabilized stearic acid as a composite phase change material for thermal energy storage, *Renewable Energy*, 2019, **140**, 862–873.
23 K. Liu, Z. Yuan, H. Zhao, C. Shi and F. Zhao, Properties and applications of shape-stabilized phase change energy storage materials based on porous material support—a review, *Mater. Today Sustain.*, 2023, **21**, 100336.
24 W. Jia, C. Wang, T. Wang, Z. Cai and K. Chen, Preparation and performances of palmitic acid/diatomite form-stable composite phase change materials, *Int. J. Energy Res.*, 2020, **44**, 4298–4308.
25 C. Li, M. Wang, Z. Chen and J. Chen, Enhanced thermal conductivity and photo-to-thermal performance of diatomite-based composite phase change materials for thermal energy storage, *J. Energy Storage*, 2021, **34**, 102171.
26 Y. Bai, Y. Gu, J. Chen and Y. Yue, A high-efficiency, salt-resistant, MXene/diatomite-modified coconut husk-based evaporator for solar steam generation, *J. Environ. Chem. Eng.*, 2024, **12**, 112282.
27 T. Xu, F. Wu, T. Zou, J. Li, J. Yang, X. Zhou, D. Liu and Y. Bie, Development of diatomite-based shape-stabilized composite phase change material for use in floor radiant heating, *J. Mol. Liq.*, 2022, **348**, 118372.
28 C. Li, M. Wang, B. Xie, H. Ma and J. Chen, Enhanced properties of diatomite-based composite phase change materials for thermal energy storage, *Renewable Energy*, 2020, **147**, 265–274.
29 P. Zhang, Y. Cui, K. Zhang, S. Wu, D. Chen and Y. Gao, Enhanced thermal storage capacity of paraffin/diatomite composite using oleophobic modification, *J. Cleaner Prod.*, 2021, **279**, 123211.
30 X. Guo, Y. Huang and J. Cao, Performance of a thermal energy storage composite by incorporating diatomite stabilized paraffin as phase change material, *Energy Build.*, 2018, **158**, 1257–1265.
31 M. Sathya and K. Pushpanathan, Synthesis and optical properties of Pb doped ZnO nanoparticles, *Appl. Surf. Sci.*, 2018, **449**, 346–357.
32 A. A. Alswat, M. B. Ahmad, T. A. Saleh, M. Z. B. Hussein and N. A. Ibrahim, Effect of zinc oxide amounts on the properties and antibacterial activities of zeolite/zinc oxide nanocomposite, *Mater. Sci. Eng. C*, 2016, **68**, 505–511.
33 X. Liu, Z. Zheng, J. Wang, Y. Wang, B. Xu, S. Zhang and J. Hou, Fluidic manipulating of printable zinc oxide for flexible organic solar cells, *Adv. Mater.*, 2022, **34**, 2106453.
34 A. U. Hasanah, P. L. Gareso, N. Rauf and D. Tahir, Photocatalytic performance of zinc oxide and metal-doped zinc oxide for various organic pollutants, *ChemBioEng Rev.*, 2023, **10**, 698–710.
35 J. Siriboon, N. Traiphol and R. Traiphol, Diacetylene-zinc (II)-zinc oxide nanocomposites for colorimetric detection of ultraviolet-A light, *ACS Appl. Nano Mater.*, 2022, **5**, 13198–13207.
36 T. Ye, C. Wang and Y. Yin, Effects of ultraviolet irradition structure and properties of nylon6, *JRRRP*, 2021, **39**(3), 35–42.
37 N. Sahan and H. Paksoy, Investigating thermal properties of using nano-tubular ZnO powder in paraffin as phase change material composite for thermal energy storage, *Composites, Part B*, 2017, **126**, 88–93.
38 X. Tong, D. Li, R. Y. A. Müslüm, Y. Wu, C. Liu and Y. Çağatay, Experimental investigation on photothermal properties of Zn–ZnO/paraffin hybrid nanofluids, *J. Therm. Anal. Calorim.*, 2023, **148**, 11029–11040.
39 J. Wang, Y. Liu and X. Zhao, Development of multifunctional porous sound-absorbing foam-coated fabric with UV resistance and heat preservation, *Text. Dyeing Finish. J.*, 2024, **46**(10), 14–20.

40 J. Zhou, J. Zhao, Y. Cui and W. Cheng, Synthesis of bifunctional nanoencapsulated phase change materials with nano-$TiO_2$ modified polyacrylate shell for thermal energy storage and ultraviolet absorption, *Polym. Int.*, 2020, **69**(2), 140–148.

41 J. Zhao, *Preparation And Properties Of Clay-Based Form-Stable Phase Change Thermal Storage Wood Plastic Composites[D]*, Beijing Forestry University, Beijing, 2022.

42 Z. Hu, S. Zheng, Y. Li, X. Wen, J. Huang and T. Huang, Effect of Calcination on Pore Structure and Fractal Characteristics of Diatomite, *J. Chin. Ceram. Soc.*, 2021, **49**, 1395–1402.

43 Z. Geng, C. Shi, Q. Zhao and L. Yang, Preparation of diatomite paraffin composite phase change coating and its simulation application in building wall, *J. Energy Storage*, 2024, **84**, 110696.

44 X. Zhang, X. Li, Y. Zhou, C. Hai, Y. Shen, X. Ren and J. Zeng, Calcium chloride hexahydrate/diatomite/paraffin as composite shape-stabilized phase-change material for thermal energy storage, *Energy Fuels*, 2018, **32**, 916–921.

45 H. Liu, D. Hu and W. Ma, Cinnamic acid-functionalized ZnO nanoparticles for constructing UV-shielding and mechanically robust polyvinyl butyral composites, *Colloids Surf.*, 2021, **629**, 127438.

46 S. Yusan, A. Bampaiti, S. Aytas, S. Erenturk and M. A. A. Aslani, Synthesis and structural properties of ZnO and diatomite-supported ZnO nanostructures, *Ceram. Int.*, 2016, **42**, 2158–2163.

47 S. Zhao, K. Sun, H. Zhang, H. Liu, D. Wu and X. Wang, Development of poly(ethylene glycol)/silica phase-change microcapsules with well-defined core-shell structure for reliable and durable heat energy storage, *Sol. Energy Mater. Sol. Cells*, 2021, **225**, 111069.

48 Y. Konuklu, O. Ersoy and O. Gokce, Easy and industrially applicable impregnation process for preparation of diatomite-based phase change material nanocomposites for thermal energy storage., *Appl. Therm. Eng.*, 2015, **91**, 759–766.

49 L. Kang, L. Ren, H. Niu, R. Lv, H. Guo and S. Bai, Paraffin@$SiO_2$ microcapsules-based phase change composites with enhanced thermal conductivity for passive battery cooling, *Compos. Sci. Technol.*, 2022, **230**, 109756.

50 T. Qian, S. Zhu, H. Wang and B. Fan, Comparative Study of Carbon Nanoparticles and Single-Walled Carbon Nanotube for Light-Heat Conversion and Thermal Conductivity Enhancement of the Multifunctional PEG/Diatomite Composite Phase Change Material, *ACS Appl. Mater. Interfaces*, 2019, **11**(33), 29698–29707.

51 D. Xu, P. Liang, X. Ying, X. Li and Q. Cheng, Development of cellulose/ZnO based bioplastics with enhanced gas barrier, UV-shielding effect and antibacterial activity, *Int. J. Biol. Macromol.*, 2024, **271**, 132335.

52 D. Kim, K. Jeon, Y. Lee, J. Seo, K. Seo, H. Han and S. B. Khan, Preparation and characterization of UV-cured polyurethane acrylate/ZnO nanocomposite films based on surface modified ZnO, *Prog. Org. Coat.*, 2012, **74**, 435–442.

53 P. Liu and Z. Su, Preparation and characterization of PMMA/ZnO nanocomposites *via in situ* polymerization method, *J. Macromol. Sci., Part B:Phys.*, 2006, **45**, 131–138.

54 C. P. Feng, K. Y. Sun, J. C. Ji, L. Hou, G. P. Cui, Z. G. Zhao and H. B. Lan, 3D Printable, form stable, flexible phase-change-based electronic packaging materials for thermal management, *Addit. Manuf.*, 2023, **71**, 103586.

55 X. Kong, R. Nie and J. Yuan, Shape stabilized three-dimensional porous SiC-based phase change materials for thermal management of electronic components, *Chem. Eng. J.*, 2023, **462**, 142168.